Origins of lasing emission in a resonance-controlled ZnO random laser

2014 New J. Phys. 16 093054

(http://iopscience.iop.org/1367-2630/16/9/093054)

New Journal of Physics
The open access journal at the forefront of physics
Deutsche Physikalische Gesellschaft DPG | IOP Institute of Physics

Origins of lasing emission in a resonance-controlled ZnO random laser

Toshihiro Nakamura[1,6], Hideki Fujiwara[2,6], Ryo Niyuki[2], Keiji Sasaki[2], Yoshie Ishikawa[3], Naoto Koshizaki[4], Takeshi Tsuji[5] and Sadao Adachi[1]

[1] Division of Electronics and Informatics, Faculty of Science and Technology, Gunma University, Kiryu, Gunma 376-8515, Japan
[2] Research Institute for Electronic Science, Hokkaido University, Sapporo, Hokkaido 001-0020, Japan
[3] National Institute of Advanced Industrial Science and Technology, Tsukuba, Ibaraki 305-8565, Japan
[4] Division of Quantum Science and Engineering, Faculty of Engineering, Hokkaido University, Sapporo, Hokkaido 060-8628, Japan
[5] Institute for Materials Chemistry and Engineering, Kyushu University, Kasuga, Fukuoka 816-8580, Japan
E-mail: nakamura@el.gunma-u.ac.jp and fuji@es.hokudai.ac.jp

Received 26 May 2014, revised 5 August 2014
Accepted for publication 27 August 2014
Published 30 September 2014

New Journal of Physics **16** (2014) 093054

doi:10.1088/1367-2630/16/9/093054

Abstract

We investigate the origins of lasing emission in a scatterer-resonance-controlled random laser made of ZnO nanopowder over a wide temperature range (20–300 K). At higher temperatures (>150 K), the lasing emission appears around exciton recombination energies and the lasing threshold carrier density is comparable to the Mott density, indicating that the resonance-controlled random laser is going toward showing excitonic lasing; at lower temperatures, random lasing is caused by usual electron–hole plasma recombination because of the threshold carrier density being much larger than the Mott density.

Keywords: ZnO, exciton, laser, random structure, Mott transition, electron–hole plasma

[6] Authors to whom any correspondence should be addressed.

1. Introduction

Random lasers have a simple structure, consisting of randomly shaped nanopowder as a scatterer and luminescent material (e.g., dye molecules [1], rare-earth ions [2] and semiconductors [3, 4]) as an optical gain material. Because of their simplicity and low cost, random lasers are attractive candidate inexpensive stimulated emission sources. Generally, random lasing arises from light amplification due to strong multiple-light-scattering events among scatterers in the gain media [5, 6]. Due to the randomness of the scattering events, however, controlling random lasing features such as the lasing wavelength and the number of spike-like peaks is very difficult. Moreover, random lasers usually have relatively large lasing thresholds due to the considerable scattering loss [3].

Random lasing from randomly shaped and sized semiconductor nanopowders (i.e., normal random lasing) occurs at the wavelength of its maximum optical gain [7], rather than at a specific resonance wavelength of the scatterer. Since the wavelength at the maximum optical gain of a semiconductor depends on the temperature, the lasing wavelength of the normal random laser gradually shifts in accordance with the temperature-dependent optical gain spectra.

We previously reported [8] that a normal ZnO random laser has a relatively large lasing threshold over a wide temperature range of T = 20–300 K due to the large scattering losses. Therefore, normal ZnO random lasing was ascribed to electron–hole plasma recombination. However, if optical losses are suppressed and the lasing threshold consequently decreases, then another lasing type, namely excitonic lasing, may dominate the random lasing process [9–11]. In fact, excitonic lasing was previously observed in GaAs quantum-wire structures in a strong carrier confinement regime [12, 13] and in a ZnO planar microcavity structure at low temperatures [14].

We proposed, in order to control the lasing modes and reduce the lasing thresholds, a new random laser structure consisting of size-monodisperse scatterers and intentionally introduced scatter-free (i.e., defect or void) sites [15, 16]. Numerical analysis demonstrated the possibility of controlling the resonant frequency, localizing the lasing position at the defect sites and realizing lasing modes with high Q [15, 16]. To experimentally verify our proposed method, we prepared a random laser from homogenized spherical ZnO nanopowder and introduced polystyrene particles as defect sites. We observed that this laser had features clearly distinct from those of normal ZnO random lasers; it exhibits quasi-single-mode lasing emissions with thresholds at room temperature much lower than those of normal ZnO random lasers [17].

In such resonance-controlled-type ZnO random lasers, the lasing characteristics are expected to depend on not only the gain properties of ZnO but also the resonance properties of the resonant scatterer. Resonance-controlled random lasers have thresholds that are an order of magnitude lower than those of normal ZnO random lasers. Therefore, a unique lasing mechanism, i.e., lasing from the exciton quasiparticles, may be realized.

In this work, we investigate the temperature dependence of the resonance-controlled ZnO random laser characteristics in order to clarify the origins of the lasing emission lines. Using the quasi-single lasing mode of the resonance-controlled ZnO random laser allows us to investigate the relation between the resonance wavelength of the scatterer and the optical gain curve, in an effort to better understand random lasing mechanisms. We showed that the lasing emission peaks appear at the resonance wavelength of the scatterer and that the lasing threshold is mainly determined by the Q-factor of the scatterer resonance mode. We discussed the origins of the

resonance-controlled lasing emission on the basis of the temperature dependence of the excited carrier densities at the lasing thresholds.

2. The experiment

We used two types of ZnO nanopowder as random lasing media: randomly shaped ZnO powder (Hakusuitec) with a mean diameter of 100 nm and spherical ZnO powder prepared by laser-induced melting of the randomly shaped ZnO powder [18, 19]. Figures 1(a) and (b) show scanning electron microscope (SEM) images of the spherical and randomly shaped ZnO powders, respectively. The mean diameter of the spherical powder was ~200 nm (figure 1(a)). These nanopowders were dispersed in distilled water. To introduce defect (scatterer-free) sites in the spherical ZnO powder system, polystyrene particles (Corefront) with a mean diameter of 900 nm were added into the spherical ZnO dispersed solution. The above solutions were then dropped onto silicon substrates and dried in air. The surface density of the defect polystyrene particles is estimated to be $\sim 1.3 \times 10^{-2}\,\mu\mathrm{m}^{-2}$.

An excitation light pulse of 355 nm with a pulse duration of 300 ps and repetition rate of 2 kHz was incident normal to the sample surface from a *Q*-switched laser (Teemphotonics). Excitation laser power losses in windows and lenses were corrected. The diameter of the excitation light spot was ~30 μm. The light emitted from the sample was collected in the same direction using a single monochromator equipped with a charge-coupled device (Princeton Instruments, PIXIS:100B) and two lenses (diameter 25 mm, focal lengths 50 and 100 mm). The spatial resolution of the present measurement system was ~7 (vertical) × 5 (horizontal) $\mu\mathrm{m}^2$, as was determined from the pixel size of the CCD and the slit width. The random lasing of the spherical ZnO powder was measured at a particular defect site (i.e., polystyrene sphere), as schematically shown in the inset of figure 1(a). A defect site was identified from a 1D image of the lasing emission using a vertical CCD array. The lasing measurements were performed at T = 20–300 K in a closed-cycle refrigerator cryostat (IWATANI CRT 105PL)[7].

3. Results and discussion

Figures 1(c) and (d) show emission spectra of spherical and randomly shaped ZnO powders, respectively, at T = 20, 180 and 300 K. For the spherical sample, each spectrum for the different temperatures was measured at different defect sites. At T = 300 K (figure 1(d)) the randomly shaped ZnO powder shows a large number of spike-like peaks, that are attributed to random lasing arising from multiple scattering in the media (i.e., commonly observed random lasing) [3]. In contrast, a single sharp peak emitted at the defect site of the spherical ZnO powder can be clearly observed in the broad spontaneous emission band (figure 1(c)). This single sharp emission peak is caused by resonant scattering of the emitted light at the spherical ZnO scatterers and by the effect of light localization around the defect site (defect-site lasing) [17]. In the defect-site lasing system, the gain is achieved by light emission from ZnO powder surrounding the defect site, and then, the localized light field is not restricted in the defect site itself but properly penetrates into the ZnO powder area. The single sharp emission peak is also

[7] Because of the limitation of our pumping laser pulse power, the lasing measurments were performed at 300 K using the experimental setup described in [17].

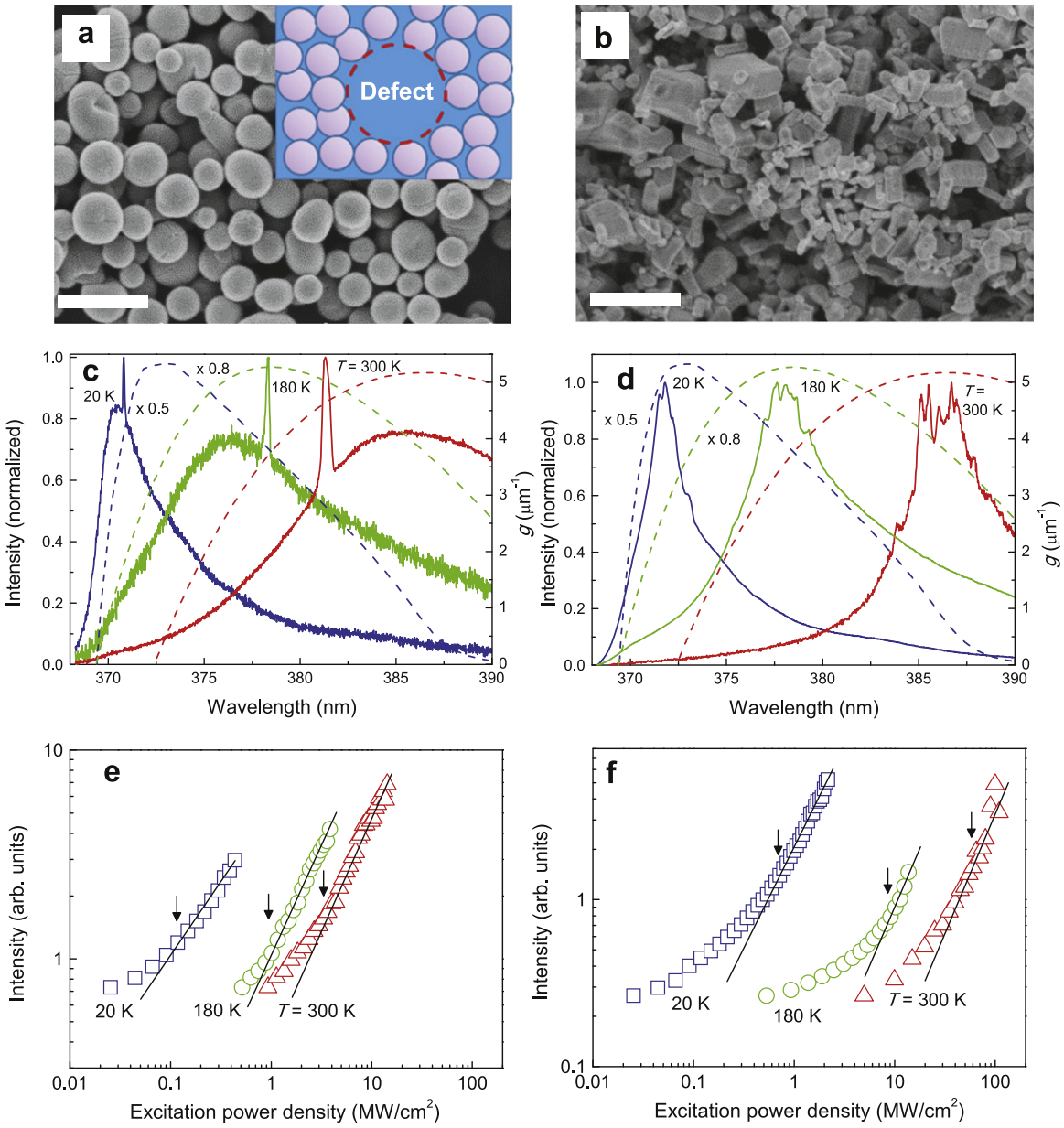

Figure 1. SEM images of (a) spherical ZnO powder and (b) randomly shaped ZnO powder. The bars indicate a length of 500 nm. The inset of (a) schematically illustrates a defect site in the ZnO powder. Emission spectra of (c) defect-site lasing and (d) normal random lasing at T = 20, 180 and 300 K. The P values in (c) are 14, 2, and 0.4 MW cm^{-2} at T = 300, 180, and 20 K, respectively. Those in (d) are 100, 14, and 2 MW cm^{-2} at T = 300, 180, and 20 K, respectively. Dashed curves in (d) represent examples of the gain spectrum g at different T (right axis). Also shown is the peak emission intensity as a function of the excitation power density for (e) defect-site lasing and (f) normal random lasing at T = 20, 180 and 300 K. The straight lines are only to guide the eye. Each vertical arrow in (e) and (f) indicates a P_{th} at which a sharp spike-like peak appears.

observed at low temperatures (T = 20 and 180 K, figure 1(c)). Such lasing peaks shift towards shorter wavelengths with decreasing T.

In previous works [7, 8], we have shown that the lasing peak position of a semiconductor (normal) random laser corresponds to the maximum of the gain spectrum calculated by using its physical parameters, not using its structural parameters. For ZnO, the optical gain spectrum $g(\omega)$ can be obtained from [22]:

$$g(w) = -\frac{2\omega}{c}\,\mathrm{Im}\left[\sqrt{1+\chi(\omega)}\right] \tag{1}$$

where c denotes the speed of light in vacuum. The optical susceptibility $\chi(\omega)$ includes the quantum many-body effects of excited carriers and can be obtained by solving the Bethe–Salpeter ladder equation which was derived from quantum field theory [22]. Details on the calculation procedure and required parameter values for $g(\omega)$ can be found in [8].

The dashed curves in figures 1(c) and (d) show, as an example, the gain spectra $g(\omega)$ at T = 20, 180 and 300 K. The peak wavelength shifts toward the shorter wavelength side with decreasing T in correspondence with the peak of normal random lasing emission. On the other hand, the lasing peak wavelengths for defect-site lasing do not always agree with the gain maximum. This indicates that the temperature dependence of the defect-site lasing peak does not follow that of the gain peak. Thus, while the peak wavelengths of a normal random laser agree with the temperature-dependent gain maximum wavelengths, those of defect-site lasing are determined by both gain and scatterer resonance properties.

Figures 1(e) and (f) show plots of the defect-site and normal random lasing *peak* emission intensities, as a function of the excitation power density P at different temperatures and at different defect sites. Here, the *peak* intensity represents the maximum in intensity of a single lasing peak (defect-site lasing) or that of a broad peak with several spikes (normal lasing). The lasing threshold power densities P_{th} for both defect-site and normal lasing decrease with decreasing T. However, P_{th} is smaller for defect-site lasing than for normal random lasing over the temperature range (i.e., P_{th} = 0.1–4.5 MW cm^{-2} for defect-site lasing and P_{th} = 0.8–65 MW cm^{-2} for normal random lasing at T = 20–300 K).

To obtain more detailed information on the defect-site lasing characteristics, the lasing spectra of the spherical ZnO powder at two different defect sites were measured at various temperatures. Figures 2(a) and (b) show the temperature-dependent defect-site lasing spectra measured at the specific defect sites A and B at the fixed excitation power densities P = 5 and 0.9 MW cm^{-2}, respectively. For comparison, figure 2(c) shows the normal random lasing spectra excited at P = 2 MW cm^{-2} at the same spot. The temperatures were varied from 300 to 220 K in figure 2(a) and from 140 to 60 K in figures 2(b) and (c).

Figure 2 shows that the lasing temperature dependence of the defect-site random laser is clearly different from that of the normal random laser. The defect-site lasing emission intensity reaches its maximum at particular temperatures: T = 260 K for A (figure 2(a)) and T = 120 K for B (figure 2(b)). In contrast, the lasing intensity for the normal ZnO random laser increases monotonically with decreasing T. The lasing wavelength for the defect-site random laser is almost temperature independent; it oscillates at ∼380 nm and ∼373 nm for A and B, respectively. The normal random laser exhibits a clear blue-shift with decreasing T according to the peak shift of the gain spectra (see also figure 1(d)).

The lasing wavelength at the defect site can be determined by the resonance frequency of the scatterer, whereas its emission intensity can be determined only by the optical gain. The

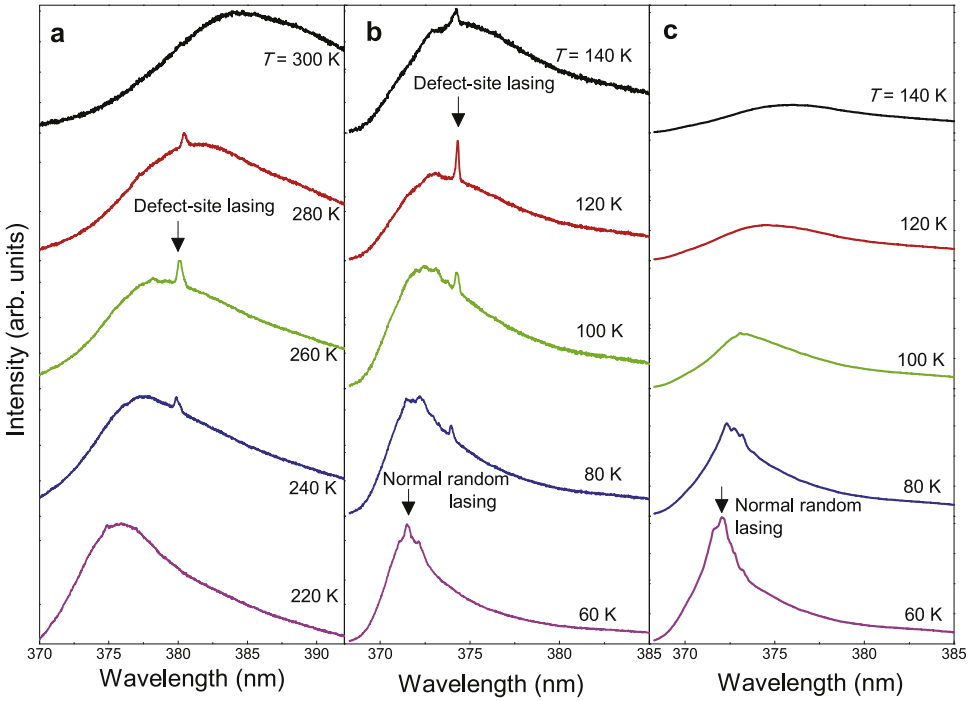

Figure 2. Lasing emission spectra of spherical ZnO powder at specific defect sites: (a) A at T = 220–300 K and (b) B at T = 60–140 K. (c) Random lasing spectra of randomly shaped ZnO powder at T = 60–140 K. The excitation power densities are (a) 5, (b) 0.9, (c) 2 MW cm^{-2}.

spectral dependence of the optical gain in semiconductors is strongly dependent on the temperature, but the resonance frequency of the scatterers is not. Therefore, the lasing emission intensity at the defect site reaches its maximum at the temperature where the optical gain at the resonance frequency of the scatterer shows the highest value. Thus, the maximum lasing emission intensities for defect sites A and B are reached at different temperatures (T = 260 and 120 K, respectively) due to the different resonance frequencies of the sites.

In figures 3(a) and (b), the defect-site lasing characteristics at different defect sites ('*non-specific*' defect sites) for temperatures from T = 20 to 300 K are shown (crosses). These data were obtained without paying attention to '*specific*' defect sites, A–D. Because the peaks of the defect lasing emission slightly blue-shifted ($\lesssim$0.5 nm) with increasing P, we employed the peak position values ($\lambda_{\rm em}$ and E_{em}) near thresholds. For comparison, the lasing position and threshold obtained from a normal random laser are also plotted. The temperature dependence of the peak position for the normal random lasing corresponds to that of the gain peak position ($E_{g,max}$ or $\lambda_{g,max}$) calculated from equation (1). At high temperatures ($T \geqslant 150$ K), the defect-site lasing wavelengths (energy) are shorter (greater) than those for the normal lasing ones. Further increasing T makes the difference more remarkable. The lasing thresholds for the defect-site lasers are much lower than those for the normal random laser when T = 20–300 K. This lasing threshold difference increases with increasing T; thus, the defect-site random laser is found to be less sensitive to the temperature than the normal random laser.

The solid curves in figures 3(a) and (b) show the lasing wavelength and threshold for four '*specific*' defect sites, A–D, plotted against T. Note that these specific defect-site lasing data

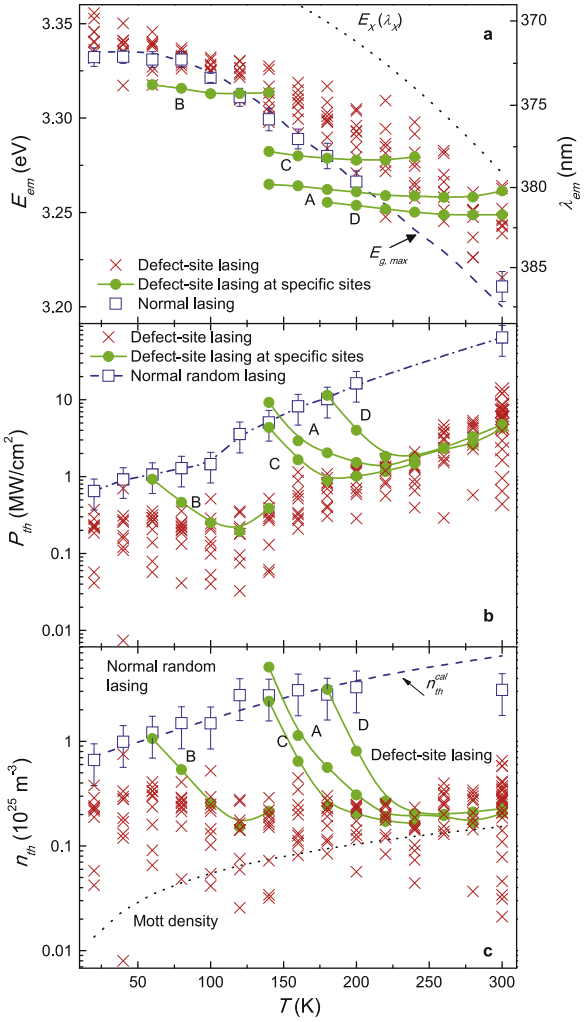

Figure 3. (a) Lasing energy (wavelength, right axis) E_{em} ($\lambda_{\rm em}$) of defect-site lasing at various defect sites (crosses) and normal random lasing (open squares) as a function of temperature T. The dashed curve represents the plots of peak energies $E_{g,max}$ in the gain spectra g. The solid circles show E_{em} ($\lambda_{\rm em}$) for defect-site lasing at specific defect sites (A–D). The dotted curve represents the exciton recombination energy (wavelength) E_X (λ_X). (b) Threshold power density P_{th} of defect-site lasing at various defect sites (crosses) and those at specific defect sites A–D (solid curves) as a function of temperature T. (c) Threshold carrier density n_{th} of defect-site lasing at various defect sites (crosses) and normal random lasing (open squares) as a function of T. The dashed curve represents the calculated threshold carrier density n_{th}^{cal}. The dotted curve shows the calculated Mott density. The solid circles show n_{th} for defect-site lasing at specific defect sites (A–D).

were obtained by lowering T from room temperature to 20 K without moving an excitation laser spot from their specific defect sites. As shown in figure 3(a), each lasing wavelength shows no strong dependence on T (e.g., it is 380 nm at A). The resonance frequency of the scatterer can be determined from the refractive index and structural size of the scatterer [15]. The smaller temperature variation of the lasing wavelength in figure 3(a) may reflect a smaller change in the refractive index of the scattered material (ZnO). The temperature variation of the refractive

index $n^{-1}(\mathrm{d}n/\mathrm{d}T)$ of semiconductors is known to be of the order of 10^{-5} (K^{-1}) [20]. The temperature dependence of the defect-site lasing threshold in figure 3(b) shows that each defect site exhibits a dip in the threshold versus T data (e.g., at $T \sim 120$ K for B). As expected, the temperature at which the lasing threshold becomes minimum corresponds to that giving the maximum lasing emission intensity (cf defect site B in figure 2(b)).

Figure 3(c) shows the threshold carrier density n_{th} (in m^{-3}) versus temperature T for the defect-site laser (crosses) together with those for the normal random laser (open squares). To carry out the conversion $P_{th} \rightarrow n_{th}$, we used the following differential equation [8]:

$$\frac{\mathrm{d}n(t)}{\mathrm{d}t} = \frac{P(t)\eta(T)}{\hbar\omega_{pl}D} - \frac{n(t)}{\tau(T)} \tag{2}$$

where $n(t)$, $P(t)$, $\hbar\omega_{pl}$ and D denote the time-dependent carrier density, the excited intensity, the photon energy of the excited light and the diameter of the ZnO nanopowder, respectively. We numerically solved equation (2) for $n(t)$ assuming a Gaussian pulse waveform [11], and then obtained n_{th} as the time-averaged value of $n(t)$ from experimental P_{th} values. The temperature-dependent parameters $\tau(T)$ and $\eta(T)$ represent the intrinsic carrier lifetime and quantum efficiency of ZnO, respectively, which were obtained from the literature (τ) [21] and from our measured spontaneous emission spectra (η). Note that the converted n_{th} values are upper limits because the reflection and/or scattering power losses due to the ZnO random laser structure are not included in the above conversion procedure. On including such power losses in the conversion procedure the density values may become lower.

In figure 3(c), we compare the experimentally determined threshold carrier densities n_{th} for a normal ZnO random laser with the theoretical carrier density n_{th}^{cal}, obtained from the gain spectra using equation (1). These calculated curves explain the experimental n_{th} of the normal random laser well, indicating that the origin of the normal random lasing is electron–hole plasma recombination [8].

We consider the temperature dependence of the defect-site lasing characteristics shown in figure 3. At temperatures below 150 K, the defect-site lasing energies agree with those of the normal random laser (figure 3(a)). Thus, the defect-site lasing mechanism at $T < 150$ K can be attributed to the electron–hole plasma recombination, like for the normal random laser [8]. Above $T \sim 150$ K, the observed lasing energies are clearly larger than those for the normal random laser and approach the exciton recombination energy (E_X) of ZnO nanoparticles [8] (dotted curve in figure 3(a)). Thus, defect-site lasing at higher temperatures ($T > 150$ K) may be related to the excitonic recombination.

As shown in figure 3(c), the n_{th} values for the defect-site lasing (crosses) are almost independent of T[8]. In more detail, the n_{th} values can be determined from the total loss in the corresponding lasing system. To achieve lasing, the optical gain, which is a quantity that is proportional to the excited carrier density, must overcome the total loss. Assuming that the loss in the present defect-site laser system is limited by the Q-factor of each localization mode, n_{th} can be directly connected with its Q value. Note that the Q-factor of the localization mode depends on the refractive index at the lasing wavelength. Thus, it has no strong dependence on

[8] This tendency is quite different from that of P_{th} in figure 2(b), where the latter shows no strong dependence on T from 20 to 300 K. The situation of there being no strong dependence of n_{th} on T obtained in figure 4(b) mainly arises from its large dependence of η (from ~1.0 at 20 K to ~0.03 at 300 K), where η is required to transform P_{th} into n_{th} (see equation (1)).

T. Although the thresholds in figure 3(b) were obtained from lasing spots at randomly selected defect sites, the n_{th} values (crosses) plotted in figure 3(c) reflect no strong dependence of the Q-factor on T. Due to there being no strong T dependence of n_{th}, the defect-site lasing peak energies fall into the range of the electron–hole ones at low temperatures ($T < 150$ K) and approach the exciton recombination energies (E_X) above ∼150 K.

In figure 3(c), the temperature dependence of n_{th} for the specific defect-site lasing case (solid circles) is quite different from that for the non-specific lasing cases (crosses). Each defect site exhibits a minimum n_{th} at different temperatures, e.g., at $T \sim 120$ K for defect site B (figure 3(c)), with no strong dependence of the lasing peak energy on T (∼3.31 eV for defect site B; figure 3(a)). Each n_{th} versus T curve in figure 3(c) exhibits a steep increase towards the side with low temperature. This behavior reflects a temperature shift of the gain spectrum of the lasing medium. In other words, because the lasing energy at specific defect sites can be determined only by their structure, i.e., their own resonance frequency [15], which has no dependence or a negligible dependence on T, n_{th} for the specific defect lasing steeply increases with decreasing T due to the large deviation between the temperature-sensitive gain maximum and the temperature-insensitive resonance energy. Note that one of the temperature-dependent loss mechanisms is an exciton–phonon coupling [8]. This loss mechanism may also lead to an increase in n_{th} for the defect-site lasing at higher temperatures.

Consequently, when we observe the lasing properties at a '*specific*' defect site and at different temperatures from higher to lower T, the lasing is initiated at a resonance frequency with a minimum n_{th} value, where the total loss and gain were balanced at the starting higher temperature. Thus, when the lasing properties are measured at different defect sites and at different temperatures (i.e., '*non-specific*' defect sites), the lasing energies shift according to their temperature-dependent gain spectra while n_{th} is almost constant over the measurement T range.

Finally, we consider the origin of our observed defect-site lasing in more detail. The Mott density can be obtained, from which the mean distance between the excitons is equal to the exciton Bohr radius. When the photoexcited carrier density exceeds the Mott density, its screening effect becomes dominant and the Coulomb attraction force becomes negligible. As a result, the exciton quasiparticles may change to exhibiting an electron–hole plasma nature. Thus, the Mott density is a criterion for distinguishing excited electronic states: excitonic or electron–hole plasma cases. The dashed curve in figure 3(c) plots the Mott density calculated using the model proposed by Versteegh *et al* [22]. For the normal random laser, the threshold carrier density (open squares) is much larger than the Mott density over the whole wavelength region, indicating electron–hole plasma lasing. The n_{th} values for different defect sites (crosses) at T below 150 K are clearly larger than the Mott density, which indicates that the defect-site lasing mechanism is due to electron–hole plasma recombination lasing. This mechanism is commonly observed in normal random lasers [8]. Above $T \sim 150$ K, on the other hand, the n_{th} values are nearly the same as the Mott density. Therefore, the defect-site lasing system approaches excitonic lasing with increasing T. This fact corresponds to the experimental evidence showing that the defect-site lasing peak at higher T appears near the exciton recombination energy (figure 3(a)).

4. Conclusion

We investigated the origins of lasing emission in artificially introduced defect sites of a spherical ZnO nanopowder random laser. Our artificially resonance-controlled random laser exhibited the usual electron–hole plasma lasing at low temperatures ($T < 150$ K). At higher T, the lasing emission appears around the exciton recombination energies and the lasing threshold carrier density becomes comparable to the Mott density, indicating that the resonance-controlled random laser system goes toward excitonic lasing with increasing T. Further tuning of the resonance of the scatterers may allow us to unambiguously show excitonic lasing. This specially designed ZnO random laser had a uniqueness, exhibiting extremely high lasing wavelength stability against temperature. The present study may thus open the possibility for realizing high performance in ZnO random lasers.

Acknowledgements

This work was partly supported by the Cooperative Research Program of the 'Network Joint Research Center for Materials and Devices' and Grants-in-Aid for Scientific Research (B) (23360133), Young Scientists (A) (22681011) and Exploratory Research (24651111) from the Ministry of Education, Culture, Sports, Science and Technology, Japan.

References

[1] Lawandy N M, Balachandran R M, Gomes A S L and Sauvain E 1994 Laser action in strongly scattering media *Nature* **368** 436–8
[2] Noginov M A 2005 *Solid-State Random Lasers* (New York: Springer)
[3] Cao H 2003 Lasing in random media *Waves Random Media* **13** 1–39
[4] Noginov M A, Zhu G, Fowlkes I and Bahoura M 2004 GaAs random laser *Laser Phys. Lett.* **1** 291–3
[5] Wiersma D S 2008 The physics and applications of random lasers *Nat. Phys.* A **4** 359–67
[6] Cao H, Zhao Y G, Ho S T, Seelig E W, Wang Q H and Chang R P H 1999 Random laser action in semiconductor powder *Phys. Rev. Lett.* **82** 2278–81
[7] Nakamura T, Takahashi T and Adachi S 2010 Temperature dependence of GaAs random laser characteristics *Phys. Rev.* B **81** 125324
[8] Nakamura T, Firdaus K and Adachi S 2012 Electron-hole plasma lasing in a ZnO random laser *Phys. Rev.* B **86** 205103
[9] Yamamoto A, Kido T, Goto T, Chen Y, Yao T and Kasuya A 1999 Dynamics of photoexcited carriers in ZnO epitaxial thin films *Appl. Phys. Lett.* **75** 469–71
[10] Priller H, Brückner J, Gruber T, Klingshirn C, Kalt H, Waag A, Ko H J and Yao T 2004 Comparison of linear and nonlinear optical spectra of various ZnO epitaxial layers and of bulk material obtained by different experimental techniques *Phys. Status Solidi* B **241** 587–90
[11] Versteegh M A M, Vanmaekelbergh D and Dijkhuis J I 2012 Room-temperature laser emission of ZnO nanowires explained by many-body theory *Phys. Rev. Lett.* **108** 157402
[12] Wegscheider W, Pfeiffer L N and Dignam M M 1993 Lasing from excitons in quantum wires *Phys. Rev. Lett.* **71** 4071–5
[13] Sirigu L, Oberli D and Degiorgi L 2000 Excitonic lasing in semiconductor quantum wires *Phys. Rev.* B **61** R10575–8
[14] Guillet T *et al* 2011 Laser emission with excitonic gain in a ZnO planar microcavity *Appl. Phys. Lett.* **98** 211105

[15] Fujiwara H, Hamabata Y and Sasaki K 2009 Numerical analysis of resonant and lasing properties at a defect region within a random structure *Opt. Express* **17** 3970–3777
[16] Fujiwara H, Hamabata Y and Sasaki K 2009 Numerical analysis of resonant properties of a waveguide structure within a random medium *Opt. Express* **17** 10522–8
[17] Fujiwara H, Niyuki R, Ishikawa Y, Koshizaki N, Tsuji T and Sasaki K 2013 Low-threshold and quasi-single-mode random laser within a submicrometer-sized ZnO spherical particle film *Appl. Phys. Lett.* **102** 061110
[18] Ishikawa Y, Feng Q and Koshizaki N 2010 Growth fusion of submicron spherical boron carbide particles by repetitive pulsed laser irradiation in liquid media *Appl. Phys.* A **99** 797–803
[19] Wang H Q, Koshizaki N, Li L, Jia L C, Kawaguchi K, Li X Y, Pyatenko A, Swiatkowska-Warkocka Z, Bando Y and Golberg D 2011 Size-tailored ZnO submicrometer spheres: bottom-up construction, size-related optical extinction, and selective aniline trapping *Adv. Mater.* **23** 1865–70
[20] Adachi S 2005 *Properties of Group-IV, III V and II VI Semiconductors* (Chichester: Wiley)
[21] Priller H, Hauschild R, Zeller J, Klingshirn C, Kalt H, Kling R, Reuss F, Kirchner C and Waag A 2005 Temperature-dependent luminescence dynamics in ZnO nanorods *J. Lumin.* **112** 173–6
[22] Versteegh M A M, Kuis T, Stoof H T C and Dijkhuis J I 2011 Ultrafast screening and carrier dynamics in ZnO: Theory and experiment *Phys. Rev.* B **84** 035207